INORGANIC CHEMISTRY FRONTIERS

RESEARCH ARTICLE

View Article Online
View Journal | View Issue

Cite this: *Inorg. Chem. Front.*, 2025, **12**, 3313

Amido/alkoxy–aryl–aryl–picolinate push–pull antennas for two-photon sensitization of Eu^{3+} luminescence†

Baptiste Chartier,[a,b] Alexei Grichine,[d] Lucile Bridou,[c] Adam Nhari,[a,b] Guillaume Micouin,[c] Akos Banyasz,[c] Didier Boturyn,[b] Jennifer K. Molloy,[b] Sule Erbek,[d,e] Véronique Martel-Frachet,[d,e] Olivier Maury *[c] and Olivier Sénèque *[a]

Luminescent two-photon (2P) absorbing lanthanide(III) complexes hold great promise for microsocpy imaging of biological samples. Conjugating such a complex to well-chosen cell penetrating peptides (CPP) allows its controlled delivery to the cytosol of live cells. However, alkoxy–phenyl–ethynyl–picolinate, one of the best antennae for 2P sensitization of Eu^{3+}, undergoes side reactions at its ethynyl group during peptide synthesis or in biological media and thus cannot be used to create such a conjugate. In this article, we evaluate the effect of substituting the ethynyl group by a phenyl one. We describe the synthesis of conjugates of the TAT CPP with Eu^{3+} complexes featuring amido–phenyl–phenyl–picolinamide, alkoxy–phenyl–phenyl–picolinamide and amido–phenyl–phenyl–picolinate ter-aryl antennae and compare their spectroscopic properties to those of analogues with bi-aryl antennae, including the amido–phenyl–picolinamide already used for 2P live cell imaging. The absorption spectrum of the ter-aryl antennae is red-shifted and better covers the active spectral range for 2P excitation by a Ti-sapphire laser. Among compounds with ter-aryl antennae, those with an amido electron donating group are the most interesting, showing brightness *ca.* 4 times higher than their bi-aryl counterparts, and similar to the ethynyl-containing antenna. 2P microscopy imaging of live cells incubated with the TAT-Eu^{3+} conjugate and dFFLIPTAT, a non-luminescent CPP that promotes cytosolic delivery, showed diffuse cytosolic staining of the Eu^{3+} probe. The ter-aryl-based probes showed superior performances compared to bi-aryl, with *ca.* 80% of the cells showing Eu^{3+} staining of the cytosol.

Received 4th February 2025,
Accepted 9th March 2025

DOI: 10.1039/d5qi00333d

rsc.li/frontiers-inorganic

Introduction

Lanthanide(III) (Ln^{3+}) complexes have luminescent properties due to f–f transitions that are very interesting for biological applications, including fine emission bands (line widths of a few nanometers) at fixed wavelengths characteristic of each lanthanide, long luminescence lifetimes and high resistance to photobleaching.[1–6] A major drawback to their use is the low efficiency of light absorption by Ln^{3+} with ε values in the order of 1–5 M^{-1} cm^{-1} for f–f transitions. This can be overcome by introducing a chromophore close to the lanthanide, capable of transferring to the lanthanide ion the energy it has acquired through light excitation, to bring it into its emissive excited state. This chromophore is called an antenna and the process of sensitizing the luminescence of the lanthanide is referred to as the antenna effect.[7–10] Sensitization of Ln^{3+} that emit in the visible (Tb^{3+}, Dy^{3+}, Eu^{3+} and Sm^{3+}) requires an antenna whose donor excited levels are above the Ln^{3+} excited emissive level (typically 2000–5000 cm^{-1} above). Consequently, for these lanthanides, it is mandatory to use antennae that are excited with UV light, which has the disadvantage of causing damage to biological samples. One solution to this problem is to use antennae that can be excited by two-photon (2P) absorption, a non-linear optical phenomenon that involves the simultaneous absorption of two photons instead of one, with half the energy required for excitation by a single photon.[11–14] As a result, the excitation is shifted from the UV to the near infrared, causing less damage to cells, for instance.

[a]*Univ. Grenoble Alpes, CNRS, CEA, IRIG, LCBM (UMR 5249), F-38000 Grenoble, France. E-mail: olivier.seneque@cea.fr*
[b]*Univ. Grenoble Alpes, CNRS, DCM (UMR 5250), F-38000 Grenoble, France*
[c]*Univ. Lyon, ENS de Lyon, CNRS UMR 5182, Laboratoire de Chimie, Lyon F-69342, France. E-mail: olivier.maury@ens-lyon.fr*
[d]*Univ. Grenoble Alpes, INSERM U1209, CNRS UMR 5309, Institute for Advanced Biosciences, F-38000 Grenoble, France*
[e]*EPHE, PSL Research University, 4-14 rue Ferrus, 75014 Paris, France*
†Electronic supplementary information (ESI) available. See DOI: https://doi.org/10.1039/d5qi00333d

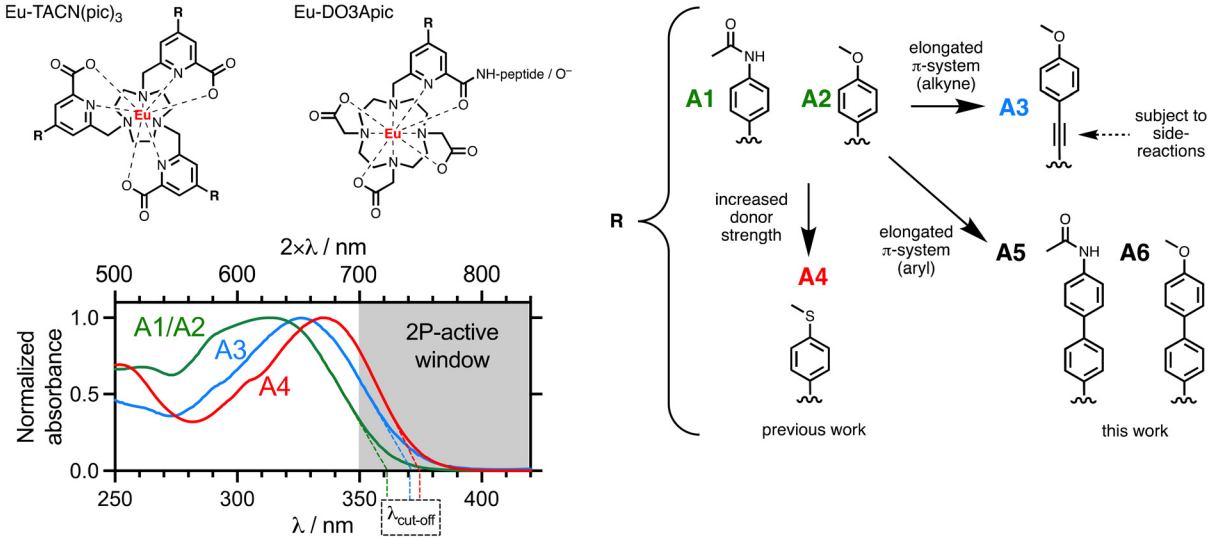

Fig. 1 Eu complexes with TACN-trispicolinate and DO3A-picolinate/picolimamide ligands, sensitizing push–pull antennas and their absorption spectra.

Over the last fifteen years, we have demonstrated that it is possible to perform 2P microscopy of fixed cells (*i.e.* cells treated with PFA or MeOH resulting in membrane permeabilization, but also causing cell death) with Ln^{3+} complexes based on a macrocyclic ligand TACN(pic)$_3$ (Fig. 1) and equipped with 2P-absorbing push–pull antennae.[13,15–17] More recently, we have used Ln^{3+} complexes based on a DO3Apic ligand equipped with a push–pull antenna and conjugated to a cell-penetrating peptide that enables the Ln complex to be delivered into the cytosol of living cells.[18–20] 2P microscopy imaging of live cells was performed using *p*-amido- or *p*-methoxy–phenyl–picolinamide antennae (A1 and A2 in Fig. 1, respectively) coordinated to the Ln^{3+}. These antennae show an absorption band in the UV (Fig. 1) with a maximum at 315 nm (λ_{max}) and that extends up *ca.* 360 nm ($\lambda_{cut\text{-}off}$). The Ti:sapphire lasers used for 2P excitation have an excitation wavelength between about 700 nm and 1050 nm, corresponding to the 350–525 nm range for 1P absorption. This means that only the tail of the absorption band of the Ln^{3+} complex is likely to be active for 2P excitation by the Ti:sapphire laser (Fig. 1). Additionally, the 2P cross-section of these antennae is small (35 GM at 700 nm for the TACN-based complex with three antennae, *i.e. ca.* 12 GM per antenna).

A better antenna is the alkoxy–phenyl–ethynyl–picolinate antenna (A3 in Fig. 1), with λ_{max} and $\lambda_{cut\text{-}off}$ values around 325 nm and 370 nm, respectively, and a 2P cross-section of *ca.* 50 GM at 700 nm.[21,22] However, its alkyne group is not completely stable and can react with nucleophiles (water, alcohols, thiols, phosphines, *etc.*) under certain conditions. For instance, under acidic conditions used during the preparation of Ln^{3+} complex-peptide conjugates (TFA treatment for protecting group removal), complete hydration of the triple bond or addition of other nucleophiles (*e.g.* the thioanisol scavenger) is observed.[18] A solution to red-shift the absorption of the aryl-picolinate antenna was recently proposed, that consists in replacing the *p*-methoxy–phenyl–ethynyl (antenna A3 in Fig. 1) substituent of the picolinate with a *p*-thioanisolyl substituent (antenna A4 in Fig. 1).[23] Such an antenna shows λ_{max} and $\lambda_{cut\text{-}off}$ values of *ca.* 330 nm and 375 nm, respectively, similar to the *p*-methoxy–aryl–ethynyl–picolinate antenna. A 2P cross-section of 35 GM at 700 nm was measured for the TACN-based complex that features three antennae. This accounts for *ca.* 12 GM per antenna. In this article, we explore an alternative solution: replacing the ethynyl linker with an aryl group. We describe the preparation and the luminescence properties of several Eu^{3+} complexes featuring *p*-amido- or *p*-methoxy–aryl–aryl–picolinamide antennae (A5 and A6 in Fig. 1, respectively), denoted here as ter-aryl antennae, in comparison with the corresponding bi-aryl *p*-amido- or *p*-methoxy–aryl–picolinamide antennae.

Results and discussion

Design and synthesis of the probes

In a previous article, we have described the conjugate mTAT [Eu·L-Ar-NHAc] (Fig. 2A). This compound comprises an Eu^{3+} ion bound to a cyclen-based macrocyclic ligand, DO3Apic, featuring a π-extended picolinamide antenna. The picolinamide moiety is substituted by a *p*-acetamido–phenyl group, in *para* position relative to the pyridine, the whole forming a bi-aryl push–pull antenna for 2P absorption. The Eu^{3+} complex is attached to a TAT peptide, which provides water solubility and cell penetration properties. Our first target probe was therefore the ter-aryl analogue mTAT[Eu·L-Ar-Ar-NHAc] (Fig. 2A). Conjugates mTAT[Eu·L-Ar-OMe] and mTAT[Eu·L-Ar-Ar-OMe] with a methoxy electron donating group instead of the acetamide group were also investigated (Fig. 2A).

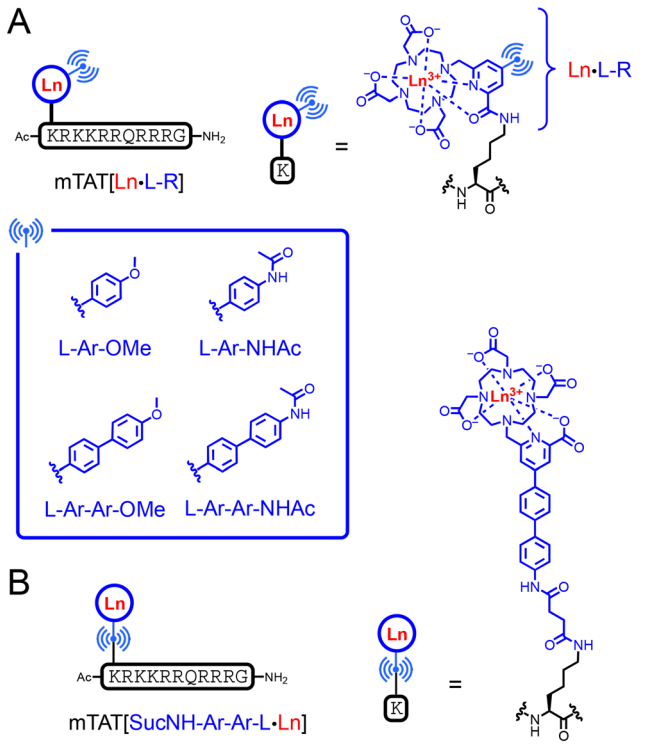

Fig. 2 Chemical structures of (A) mTAT[Ln·L-R] conjugates (R = Ar-OMe, Ar-NHAc, Ar-Ar-OMe and Ar-Ar-NHAc; Ln = Eu^{3+} or Gd^{3+}) and (B) the mTAT[SucNHArArL·Ln] conjugate.

The three new probes were synthesized as already reported for mTAT[Eu·L-Ar-NHAc].[19] The iodinated compound **1** (Fig. 3A) was engaged in a Miyaura–Suzuki coupling with borylated aromatics **3b–d** to yield pro-ligands L-R(tBu)$_3$ after hydrolysis of the picolinic methyl ester. All pro-ligands were obtained in similar yields (34–48%) after HPLC purification. Preparation of the conjugates was performed as already described.[19] L-R(tBu)$_3$ pro-ligands were then coupled to the selectively deprotected lysine side chain of the peptide, on resin using PyBOP/DIEA activation (Fig. S6 of ESI†). The peptide was cleaved from the resin and all protecting groups, including the macrocyclic ligand tBu ones, were removed by TFA/scavenger treatment for 4 h. The conjugates were purified by HPLC and metalation with Eu^{3+} was performed in water at pH 8 in the presence of excess $EuCl_3$ to give mTAT[Eu·L-Ar-OMe], mTAT[Eu·L-Ar-Ar-NHAc] and mTAT[Eu·L-Ar-Ar-OMe] as pure compounds after HPLC purification as attested by LCMS analysis (Fig. S8 of ESI†).

Due to the disappointing luminescence properties of mTAT [Eu·L-Ar-Ar-NHAc] and mTAT[Eu·L-Ar-Ar-OMe] (*vide infra*), we have also investigated the influence of the peptide anchoring position onto the complex. For this purpose, mTAT[SucNH-Ar-Ar-L·Eu] was prepared, in which the ter-aryl antenna is attached to the peptide through the electron donating group rather than through the picolinate moiety. This results in a negatively charged Eu^{3+} complex with a picolinate coordinating group rather than a neutral complex with a picolinamide

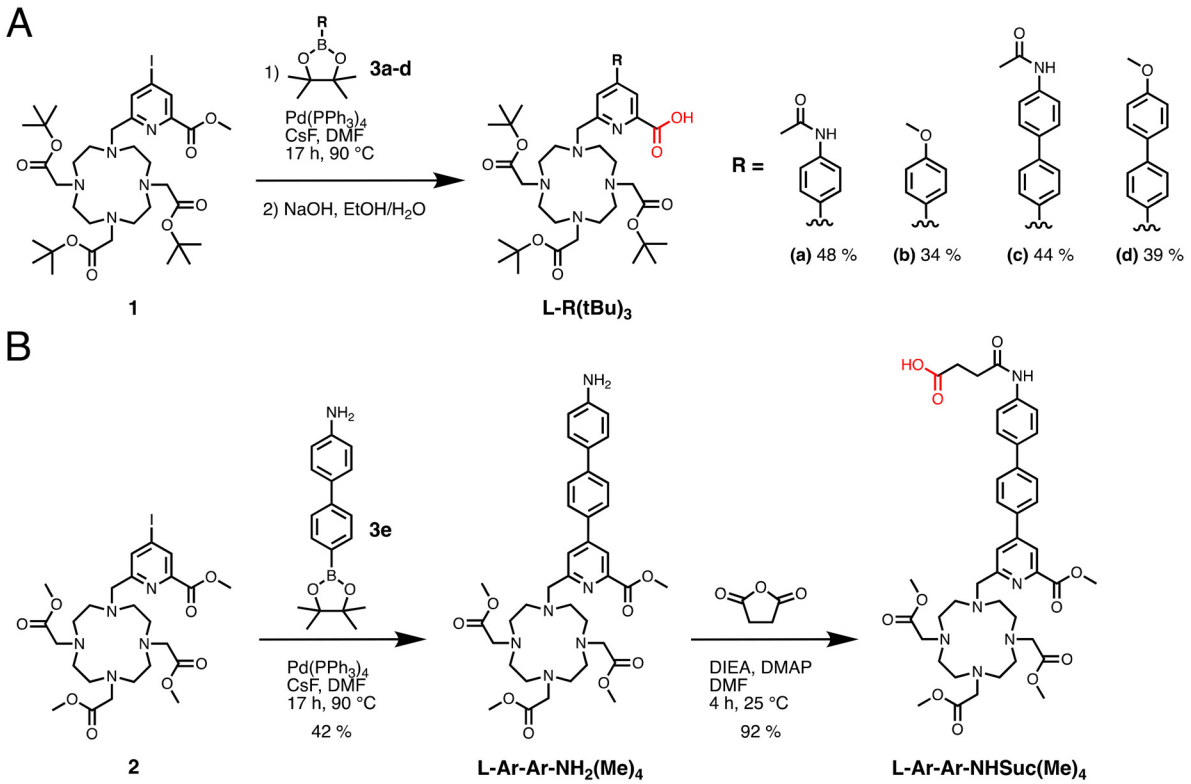

Fig. 3 Synthetic pathways for pro-ligands (A) L-R(tBu)$_3$ (R = Ar-NHAc,[19] Ar-OMe, Ar-Ar-NHAc and Ar-Ar-OMe) and (B) L-Ar-Ar-NHSuc(Me)$_4$. The carboxylic acid group used for peptide conjugation is highlighted in red.

group (Fig. 2). The synthesis of the pro-ligand L-Ar-Ar-NHSuc $(Me)_4$ and its TAT conjugate were performed starting from the iodinated compound **2**. It was coupled to boronic ester **3e** to form L-Ar-Ar-$NH_2(Me)_4$, followed by treatment with succinic anhydride to give pro-ligand L-Ar-Ar-NHSuc$(Me)_4$ (Fig. 3B), which was then coupled to the mTAT peptide on resin (Fig. S7 of ESI†). After resin cleavage in TFA and HPLC purification, the methyl protecting groups of the carboxylates were removed using a NaOH 2 M treatment for 15 minutes prior to metalation with $EuCl_3$ in water, which gave mTAT[SucNH-Ar-Ar-L·Eu].

Photophysical properties

The photophysical properties of these probes were investigated in PBS buffer (pH 7.4). Spectroscopic data are summarized in Table 1.

Absorption. All compounds show a strong absorption in the UV assigned to an intra-ligand charge transfer (ILCT) transition within the antenna. The absorption spectra of the two probes with bi-aryl antennas, mTAT[Eu·L-Ar-NHAc] and mTAT [Eu·L-Ar-OMe], are almost identical with maximum and cut-off wavelengths at *ca.* 316 nm and 365 nm, respectively (Fig. 4A and B). In comparison with the bi-aryl compounds, their two ter-aryl analogues, mTAT[Eu·L-Ar-Ar-NHAc] and mTAT[Eu·L-Ar-Ar-OMe] have red-shifted absorption, *ca.* 15 and 20 nm, respectively (Fig. 4A). The former has a higher molar absorption. The third ter-aryl-based compound, mTAT[SucNH-Ar-Ar-L·Eu], anchored through the electron-donating group, is also red-shifted compared to the bi-aryl compounds but less than the two other ter-aryl compounds (Fig. 4A), but it presents the highest molar absorption among ter-aryl compounds (Fig. 4A and Table 1). Therefore, all ter-aryl compounds have a λ_{max} around 330 nm (±5 nm), close to the ones displayed by *p*-alkoxyphenyl–ethynyl–picolinate and thioanisolyl–picolinate antennas. Interestingly, at 350 nm and above, the absorption of the three ter-aryl compounds is very similar and significantly higher than the bi-aryl ones.

Eu^{3+} emission. All five compounds show a characteristic Eu^{3+} emission with bands at 580, 590, 615, 650 and 700 nm corresponding to the $^5D_0 \rightarrow {}^7F_J$ transitions (J = 0–4) when excited into the ILCT band (Fig. 4B and Fig. S9†). Emission spectra of Eu^{3+} complexes are known to be very sensitive to the coordination sphere.[24] The five Eu^{3+} emission spectra are very similar. This is in agreement with an identical N_5O_4 coordination environment forced by the DO3Apicolinamide/picolinate ligand. Indeed, the *para* substituent of the picolinate group has only minimal effect on the coordination and on the Eu^{3+} emission spectrum. In all cases, the excitation spectrum (Fig. S9†) matches well the absorption spectrum indicating Eu^{3+} sensitization through the ILCT band of the antenna. While the conjugates with the bi-aryl antennae, mTAT[Eu·L-Ar-NHAc] and mTAT[Eu·L-Ar-OMe], have an Eu^{3+} emission quantum yield, Φ_{Eu}, of 0.15 and an Eu^{3+} emission lifetime, τ_{Eu}, of 1.05 ms, their ter-aryl analogues, mTAT[Eu·L-Ar-Ar-NHAc] and mTAT[Eu·L-Ar-Ar-OMe], show significantly lower quantum yields (0.075 and 0.035, respectively, Table 1 and Fig. S10†) and shorter emission lifetimes (0.7 and 0.4 ms,

Table 1 Spectroscopic characterizations in PBS pH 7.4[a]

Compound	λ_{max}; $\lambda_{cut\text{-}off}$/nm	$E(S_1)$;[b] $E(T_1)$[c]/cm^{-1}	ε at λ_{max}/M^{-1} cm^{-1}	Φ_{Eu}	Φ_{Eu}^{Eu}	η_{sens}	σ_{2P} at 720 nm/GM	B_{2P} at 720 nm/GM	τ_{Eu} (H_2O, aerated); τ_{Eu} (H_2O, de-oxygenated); τ_{Eu} (D_2O, aerated)/ms	τ_R/ms
mTAT[Eu·L-Ar-NHAc]	315; 366	S_1: 27 300; T_1: 22 000	20 000	0.15	0.22	0.67	5.3	0.8	1.05; 1.05; 1.63	4.68
mTAT[Eu·L-Ar-OMe]	318; 364	S_1: 27 500; T_1: 22 000	21 000	0.15	0.22	0.67	3.5	0.5	1.05; 1.05; 1.65	4.56
mTAT[Eu·L-Ar-Ar-NHAc]	329; 384	S_1: 26 000; T_1: 20 400	29 000	0.075	0.16	0.48	33	2.5	0.71; 0.76; 0.99	4.56
mTAT[Eu·L-Ar-Ar-OMe]	333; 390	S_1: 25 600; T_1: 20 400	24 000	0.035	0.086	0.41	41	1.4	0.39 (93%), 0.77 (7%); 0.40 (92%), 0.78 (8%); 0.46 (89%), 0.89 (11%)	4.56
mTAT[SucNH-Ar-Ar-L·Eu]	326; 381	S_1: 26 300; T_1: 20 700	34 000	0.15	0.22	0.67	24	3.6	1.02 1.03 1.51	4.54

[a] Error is estimated ±5% on ε values and ±10% on Φ_{Ln} and σ_{2P}. Error on τ_{Ln} is estimated ± 0.03 ms. [b] Energy of the excited singlet state is determined from the $\lambda_{cut\text{-}off}$. [c] Energy of the excited triplet state is estimated from the wavelength at half-maximum on the onset of the time-gated phosphorescence spectrum of the Gd^{3+} analogue in PBS/glycerol 9 : 1 v/v recorded at 77 K.

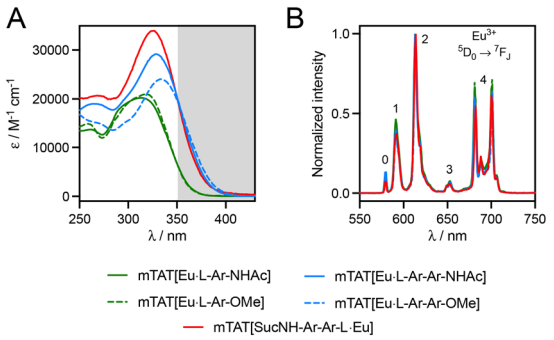

Fig. 4 1P Spectroscopic characterization of mTAT[Eu·L-R] (R = Ar-AcNH, Ar-OMe, Ar-Ar-NHAc and Ar-Ar-OMe) and mTAT[SucNH-Ar-Ar-L·Eu] probes in PBS: (A) Absorption spectra, (B) normalized emission spectra (λ_{ex} = 315 nm for mTAT[Eu·L-Ar-NHAc] and mTAT[Eu·L-Ar-OMe] and 330 nm for the others) recorded in PBS pH 7.4.

respectively, Table 1). The shorter lifetime indicates an additional non-radiative de-excitation pathway for the Eu^{3+} excited state of the latter two, while the lower quantum yield is the result of either a lower sensitization efficiency of the antenna or an additional de-activation pathway or both. Strikingly, mTAT[SucNH-Ar-Ar-L·Eu] shows Eu^{3+} emission quantum (0.15) and lifetimes (1.02 ms) almost identical to those of the bi-aryl compounds.

Mechanistic insights. Common pathways for Ln^{3+} excited states de-activation are energy transfer to the overtones of O–H vibrations, especially those of coordinated water molecules, and back energy transfer to the antenna excited triplet states.[1,8] In order to gain more insight into the deactivation mechanism, the number of coordinated water molecules, q, and the excited triplet state energy were determined. Regarding q, the Eu^{3+} emission lifetimes were measured in PBS buffer prepared with H_2O and D_2O (Table 1) and q was determined from Parker's equation $q = 1.2 \times (1/\tau_{Eu}(H_2O) - 1/\tau_{Eu}(D_2O) - c)$ with τ_{Eu} in ms and with $c = 0.325$ to account for the picolinamide ligands, which includes a coordinated CONHR group (Table S1†).[25] In all cases, the q value was zero (Table S1†), confirming that the DO3Apicolinamide ligand saturates Eu^{3+}, whatever the antenna, in agreement with the similarity of the Eu^{3+} spectra. The excited triplet state energy was determined from the emission spectra at 77 K of Gd^{3+} analogue in frozen PBS/glycerol 9/1 mixture (Fig. S11†). The triplet state of mTAT[Eu·L-Ar-Ar-NHAc] and mTAT[Eu·L-Ar-Ar-OMe] are *ca.* 1500 cm^{-1} lower than those of their bi-aryl counterparts but *ca.* 3000 cm^{-1} higher than the Eu^{3+} $^5D_0$ excited state. Such an energy gap precludes any back energy transfer from the Eu^{3+} $^5D_0$ state to the antenna triplet state, which is also confirmed by the absence of O_2 sensitivity of the Eu^{3+} emission lifetime (Table 1). The additional de-activation processes at play in mTAT[Eu·L-Ar-Ar-NHAc] and mTAT[Eu·L-Ar-Ar-OMe] are not due to additional coordinated water molecules or a low-lying triplet state and remain unexplained.

In the case of Eu^{3+}, the metal-centred emission quantum yield (Φ_{Eu}^{Eu}, also named intrinsic quantum yield) can be determined from the emission spectrum using eqn (1) and (2), where τ_R is the radiative lifetime of Eu^{3+}, n is the refractive index of the medium, I_{tot} and I_{MD} are the total area of the corrected Eu^{3+} emission spectrum and the area of the $^5D_0 \rightarrow {}^7F_1$ transition band, respectively, and $A_{MD,0}$ is the spontaneous emission probability for the $^5D_0 \rightarrow {}^7F_1$ transition.[26] $A_{MD,0}$ was initially assumed to be constant and equal to 14.65 s^{-1},[26] but significant deviations from this value were recently reported.[27] Therefore, these equations have to be used with caution when comparing complexes. Nevertheless, (i) as all the complexes described here are based on the DO3Apic chelator, (ii) as they have nearly identical emission spectra and (iii) as they have the same hydration state (q = 0), the derived τ_R and Φ_{Eu}^{Eu} values can be compared. Their values are given in Table 1.

$$\Phi_{Eu}^{Eu} = \tau_{Eu}/\tau_R \quad (1)$$

$$1/\tau_R = A_{MD,0} \times n^3 \times (I_{tot}/I_{MD}) \quad (2)$$

In agreement with their nearly identical emission spectra, all compounds have the same τ_R value, *ca.* 4.6 ms, and the differences in their intrinsic quantum yield values follow the differences in the τ_{Eu} values.

The sensitizing efficiency, η_{sens}, which quantifies the efficiency of the electronic energy transfer from the antenna to the Eu^{3+}, can be calculated from eqn (3).

$$\Phi_{Eu} = \eta_{sens} \times \Phi_{Eu}^{Eu} \quad (3)$$

The conjugates with the bi-aryl antennae, mTAT[Eu·L-Ar-NHAc] and mTAT[Eu·L-Ar-OMe], show the same sensitization efficiency, 0.67, but their ter-aryl analogues, mTAT[Eu·L-Ar-Ar-NHAc] and mTAT[Eu·L-Ar-Ar-OMe], show significantly lower η_{sens} values, *i.e.* 0.48 and 0.41, respectively. With push–pull antennas, photoinduced electron transfer (PeT) from the excited antenna to the Eu^{3+} is likely to compete with the electronic energy transfer.[20,28] The Gibbs energy of the PeT process can be evaluated using eqn (4).[29–33]

$$\Delta G_{eT}^0 = (E_D^0 - E_A^0) - E^* + \Delta G_{S+C} \quad (4)$$

where E_D^0 is the oxidation potential of the electron donor (anisole or acetanilide moieties), E_A^0 is the reduction potential of the acceptor (Eu^{3+}), E^* is the excited state energy of the antenna, *i.e.* $E(S_1)$ in Table 1. The last term accounts for solvation and coulombic interactions within the donor/acceptor pair after electron transfer. It can be estimated *ca.* −0.15 eV.[31–33] The oxidation potential of anisole and acetanilide donors were determined at E_{ox}^0 = 1.8 and 1.9 V per NHE by cyclic voltammetry measurements using *N*-(4′-iodo-[1,1′-biphenyl]-4-yl)acetamide and 4-bromo-4′-methoxy-1,1′-biphenyl as model compounds, in line with values reported in the literature.[34] The reduction potential of Eu^{3+} bound to the DO3Apicolinamide chelator has been determined at −1.2 V per NHE. From the $E(S1)$ values in Table 1, we can calculate that −0.6 eV < ΔG_{eT}^0 < −0.3 eV for the mTAT[Eu·L-R] conjugates, indicating that PeT is possible within these compounds. A difference in the rate constants of the PeT and the energy

transfer processes may explain the difference observed in η_{sens} within this family. A PeT process between the excited Eu^{3+} and the antenna can also happen. The Gibbs energy of such a process can be calculated taking for E^* the energy of the $^5D_0$ state of Eu^{3+}, *i.e.* 2.14 eV. In this case, $\Delta G^0_{eT} > 0.6$ eV, indicating that such a PeT process is not possible and cannot be involved in the de-activation of the Eu^{3+} $^5D_0$ excited state. Therefore, a PeT process may be responsible for the lower η_{sens} in mTAT[Eu·L-Ar-Ar-NHAc] and mTAT[Eu·L-Ar-Ar-OMe] but not for the lower τ_{Eu}, which remains to be clarified.

Influence of the peptide anchoring point. At this stage, we reasoned that the efficiency of PeT process could be lowered by shifting from a neutral Eu^{3+} complex to an anionic one. Indeed, it has been demonstrated that the reduction potential of Eu^{3+} decreases by *ca.* 100 mV replacing an amide by a carboxylate in the coordination sphere.[28] This prompted us to move the peptide anchoring point on the complex to the electron donating group of the antenna in order to have a picolinate instead of a picolinamide in the Eu^{3+} coordination sphere and thus we designed mTAT[SucNH-Ar-Ar-L·Eu]. Interestingly, this modification restores both a high sensitization efficiency (η_{sens} = 0.67) and a long Eu^{3+} emission lifetime (τ_{Eu} = 1.05 ms), comparable to those of the bi-aryl antennae. Consequently, mTAT[SucNH-Ar-Ar-L·Eu] is the most interesting ter-aryl compound: its absorption is red-shifted compared to the bi-aryl compounds but its overall quantum yield remains unchanged (Φ_{Eu} = 0.15).

Two-photon absorption. The 2P-absorption properties of the conjugates were studied in PBS using the two-photon excited fluorescence method with a Ti:sapphire laser source. When the conjugates in PBS solution are excited at 730 nm with the Ti:sapphire laser, the Eu^{3+} emission is detected with a quadratic dependence of its intensity on the laser power, which confirms biphotonic excitation (Fig. 5A). The 2P absorption spectra are show in Fig. 5B and compared to the 1P absorption spectrum in Fig. S12.† For all compounds, an excellent agreement is observed between the wavelength-doubled 1P absorption spectrum and the 2P absorption spectrum above 680 nm. This indicates that the ILCT transition of the antenna that is responsible for Eu^{3+} sensitization is 2P allowed as expected for non-centrosymmetric compounds. At 720 nm, the excitation wavelength used in 2P microscopy experiments (*vide infra*), the 2P cross-sections (σ_{2P}) of the three ter-aryl-based compounds are much higher than those of the bi-aryl ones (24–41 GM *vs.* 3.5–5.3 GM, respectively), showing a significant improvement of the 2P absorption efficiency by extending the antenna with a phenyl group. Among ter-aryl compounds, mTAT[Eu·L-Ar-Ar-OMe] has the highest σ_{2P} and mTAT[SucNH-Ar-Ar-L·Eu] the lowest. However, taking into account the Eu^{3+} emission quantum yields, the reversed trend is observed concerning the 2P brightness, $B_{2P} = \sigma_{2P} \times \Phi_{Eu}$ (Table 1). The cross-section values at 720 nm of the three ter-aryl compounds are comparable to those determined for the alkoxy–phenyl–ethynyl–picolinate antenna (antenna A3 in Fig. 1, *ca.* 35 GM per antenna at 720 nm) and higher than those of the thioanisolyl–picolinate antenna (antenna A4 in Fig. 1, *ca.* 8 GM per antenna at 720 nm) in related Eu^{3+} complexes. This demonstrates that the replacement of the ethynyl group by a phenyl in alkoxy–phenyl–ethynyl–picolinate antennas is a valuable solution to reactivity issues encountered with the alkyne group.

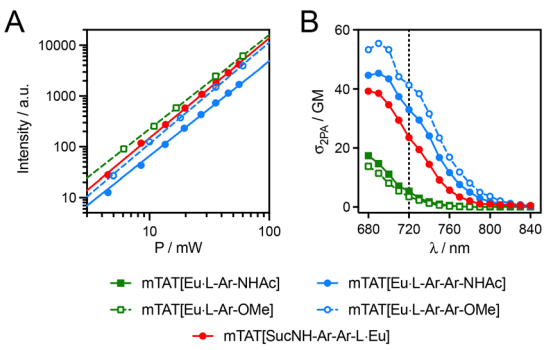

Fig. 5 2P spectroscopy: (A) quadratic power dependence of the Eu^{3+} emission (λ_{ex} = 730 nm) for mTAT[Eu·L-R] (R = Ar-OMe, Ar-Ar-NHAc and Ar-Ar-OMe) and mTAT[SucNH-Ar-Ar-L·Eu] in PBS. Data were fitted using $I = A \times P^n$ yielding n = 1.85, 1.87, 1.99 and 1.97, respectively. (B) 2P absorption spectra measured in PBS. The vertical dotted line corresponds to the 2P excitation wavelength used for cell microscopy imaging. Measurements were performed in PBS pH 7.4.

Two-photon microscopy

The mTAT conjugates with the ter-aryl antennae and an amido electron donating group showed better emission properties compared to the one with a methoxy group. Therefore, two-photon microscopy (2PM) on live HeLa cells was attempted with conjugates featuring complexes [Eu·L-Ar-NHAc], [Eu·L-Ar-Ar-NHAc] and [SucNH-Ar-Ar-L·Eu]. We were interested to know if cytosolic delivery of the Eu^{3+} probe could be achieved with these conjugates. 2P excitation was performed at 720 nm and emission was collected with an avalanche photodiode (APD) for better sensitivity or an array of photomultipliers (PMT) to achieve spectral detection. Under 720 nm 2P excitation, the main contributors to the emission are the Eu^{3+} probe and the cell autofluorescence arising from 2P-excited NAD(P)H and FAD.[19,35–37] Cell autofluorescence mostly originates from mitochondria and has a perinuclear distribution. It is characterized by a broad emission with a maximum at *ca.* 480 nm extending up to 620 nm (Fig. 6B). The fine Eu^{3+} $^5D_0 \rightarrow {}^7F_J$ emission bands at 595 nm (J = 1) and 615 nm can easily be discriminated from the cell autofluorescence by spectral detection.

mTAT probes. HeLa cells were incubated 1 h with the mTAT[Eu·L-Ar-Ar-NHAc] and mTAT[SucNH-Ar-Ar-L·Eu] at 5 μM. Both compounds behaved very similarly. Fig. 6 shows the 2PM images obtained for the latter. As shown in Fig. 6A, the majority of cells show dominant perinuclear emission but some cells also show a faint diffuse emission in the entire cell, including the nucleus. Spectral detection revealed that both autofluorescence and Eu^{3+} signals are present. Linear unmixing of both spectral components shows that the perinuclear emission is autofluorescence while the diffuse emission corresponds to Eu^{3+}, which is overall very weak (Fig. 6B).

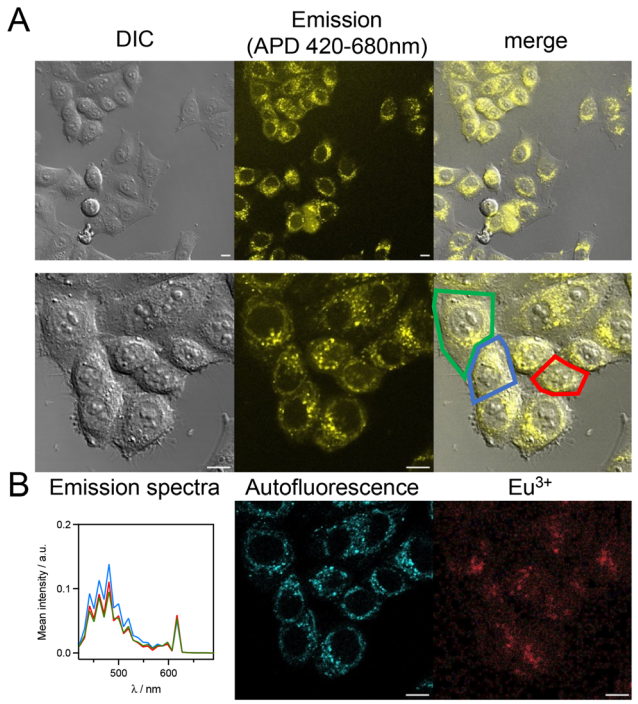

Fig. 6 2PM imaging (λ_{ex} = 720 nm) of living HeLa cells incubated 1 h with mTAT[SucNH-Ar-ArL·Eu] (5 μM) in RPMI medium. (A) Left panel: differential interference contrast (DIC) image; Middle panel: luminescence image recorded with 420–680 nm bp APD detection (arbitrarily coloured in yellow); Right panel: merge. Scale bars correspond to 10 μm. (B) Left panel: 2P-excited emission spectra (detected with a PMT array and averaged over the whole cell surface) of the cells outlined in red, blue and green in panel A; Middle and right panels: autofluorescence and Eu^{3+} emission maps obtained by linear unmixing of a 2P-excited spectral image recorded with the PMT.

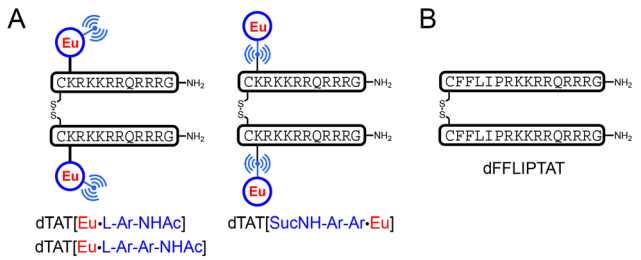

Fig. 7 Chemical structures of (A) luminescent Eu^{3+} probes based on a dimeric TAT peptide and (B) non luminescent dimeric TAT derivative dFFLIPTAT.

Dimeric TAT (dTAT) probes. Inspired by the work of Pellois,[38] we have shown by 2PM that dTAT[Ln·L] conjugates (Ln = Tb and Eu), comprising two Ln^{3+} complexes bound to a TAT dimer, efficiently reach the cytosol of living cells and give 2PM images with intense and diffuse Ln^{3+} emission within the entire cell.[19] Hence, we prepared compounds dTAT[Eu·L-Ar-Ar-NHAc] and dTAT[SucNH-Ar-Ar-L·Eu] in order to evaluate their ability to stain the cytosol of live cells (Fig. 7A and ESI† for synthesis details).

First, we examined their cytotoxicity on HeLa cells by the MTT proliferation assay in order to evaluate the concentration that could be used for 2PM experiments. While the previously described dTAT[Eu·L-Ar-NHAc] conjugate was not cytotoxic up to 20 μM (IC50 > 50 μM), both dTAT[Eu·L-Ar-Ar-NHAc] and dTAT[SucNH-Ar-Ar-L·Eu] were found to be more toxic (Fig. 8A), with an IC50 of 6 ± 1 and 12 ± 2 μM, respectively. This was not unexpected since we have observed that a higher antenna hydrophobicity in these compounds causes higher cytotoxicity.[19,20] From the MTT assays, we found that the maximal nontoxic concentration that could be used for dTAT [Eu·L-Ar-Ar-NHAc] and dTAT[SucNH-Ar-Ar-L·Eu] is 2.5 μM. 2PM was performed on HeLa cells incubated 1 h with the probes at 2 μM. With dTAT[SucNH-Ar-Ar-L·Eu], an intense punctate emission was observed within the cell (Fig. 8B and Fig. S13 of ESI†), which was assigned to Eu^{3+} emission by spectral detection (Fig. 8C). dTAT-based probes were shown to accumulate in endosomes when incubated at a concentration ≤2.5 μM.[19,38] Although co-localization with an endo/lysosome tracker was not attempted here, it is likely to be the case here again. A similar staining was obtained with dTAT[Eu·L-Ar-Ar-NHAc]. Therefore, the dTAT strategy is not pertinent for ter-aryl antennae in order to achieve cytosolic delivery.

mTAT probes co-incubated with dFFLIPTAT. More recently, we have shown that the internalization of a related probe, mTAT[Eu·L-Ar-Cz],[20] with a *N*-carbazolyl–phenyl–picolinamide antenna, could be boosted by co-incubation with the

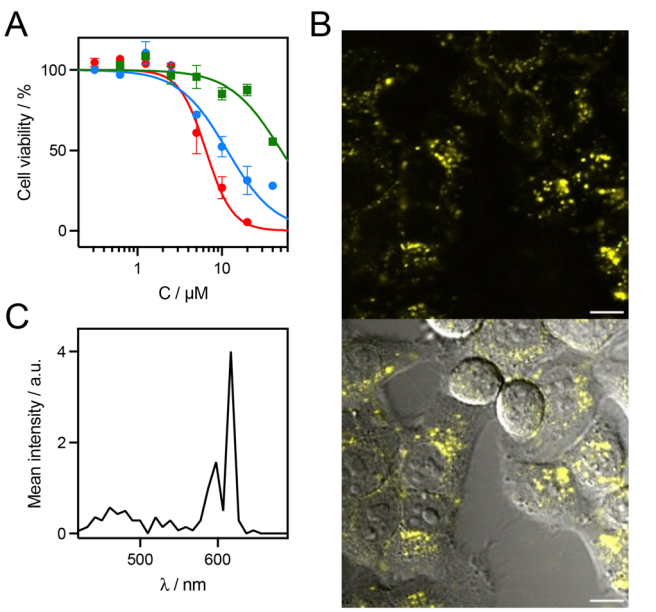

Fig. 8 (A) MTT proliferation assays performed on HeLa cells with dTAT [Eu·L-Ar-NHAc] (green),[19] dTAT[Eu·L-Ar-Ar-NHAc] (blue) and dTAT [SucNH-Ar-Ar-L·Eu] (red). (B) 2PM imaging (λ_{ex} = 720 nm) of HeLa cells incubated 1 h with dTAT[SucNH-Ar-Ar-L·Eu] (2 μM) in RPMI medium, showing (top) the luminescence image recorded with 420–680 nm bp APD detection and (bottom) the superimposition of DIC and luminescence images. (C) Typical emission spectrum emanating from puncta. Scale bars correspond to 10 μm.

dFFLIPTAT peptide, a non-luminescent TAT dimer introduced by Pellois (Fig. 7B).[39] This peptide was reported as an endosomolytic agent, that makes co-incubated species reach the cytosol. This strategy was tested with mTAT[Eu·L-Ar-NHAc], mTAT[Eu·L-Ar-Ar-NHAc] and mTAT[SucNH-Ar-Ar-L·Eu]. Prior to 2PM, a MTT proliferation assay was performed in order to assess the toxicity of mixtures of dFFLIPTAT (1.5 μM) and the conjugates (5 μM). Cells incubated for 1 h with dFFLIPTAT alone at 1.5 μM showed good viability (*ca.* 90%).[20,39] In co-incubation experiments, the cell viability was similar (Fig. S14 of ESI†), indicating that the mTAT conjugates do not increase toxicity. Therefore, incubation of HeLa cells was performed with a mixture of dFFLIPTAT (1.5 μM) and mTAT[Eu·L-Ar-NHAc], mTAT[Eu·L-Ar-Ar-NHAc] or mTAT[SucNH-Ar-Ar-L·Eu] (5 μM) for 1 h and the 2P imaging properties of the three probes were compared.

Fig. 9A shows typical images obtained with mTAT [SucNH-Ar-Ar-L·Eu] in co-incubation with dFFLIPTAT. Contrarily to images obtained with the mTAT[SucNH-Ar-Ar-L·Eu] probe alone (Fig. 6), those obtained with dFFLIPTAT, show a majority of cells with dominant diffuse emission. In many cells, the perinuclear distribution characteristic of autofluorescence is hardly identified, hidden by the intense diffuse emission. Spectral detection (Fig. 9B) confirmed that the latter corresponds to Eu^{3+}. Comparison of Fig. 6 and 9 clearly indicates that dFFLIPTAT boosts the internalization of the Eu^{3+} probe.

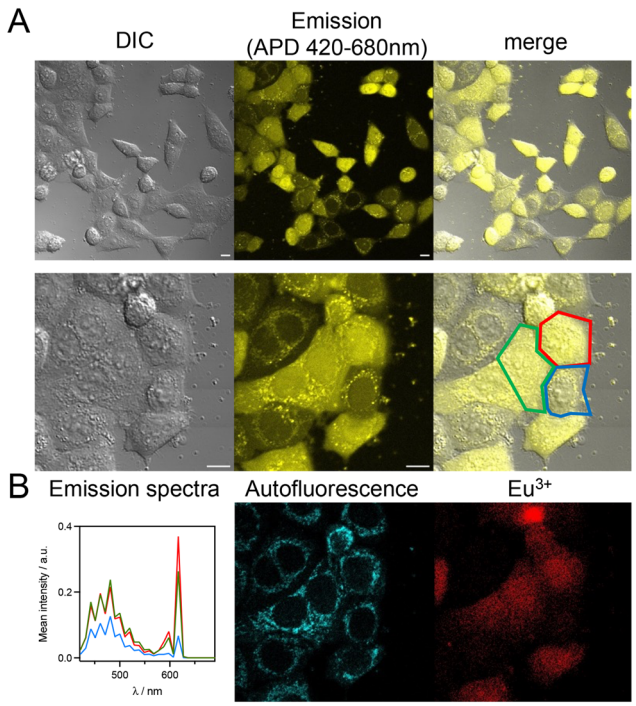

Fig. 9 2PM imaging (λ_{ex} = 720 nm) of living HeLa cells incubated 1 h with mTAT[SucNH-Ar-ArL·Eu] (5 μM) and dFFLIPTAT (1.5 μM) in RPMI medium. (A) Left panel: DIC image; Middle panel: luminescence image recorded with 420–680 nm bp APD detection (arbitrarily coloured in yellow); Right panel: merge. Scale bars correspond to 10 μm. (B) Left panel: 2P-excited emission spectra (detected with a PMT array and averaged over the whole cell surface) of the cells outlined in red, blue and green in panel A; Middle and right panels: autofluorescence and Eu^{3+} emission maps (coloured in cyan and red, respectively) obtained by linear unmixing of a 2P-excited spectral image recorded with the PMT.

The three mTAT[Eu·L-Ar-NHAc], mTAT[Eu·L-Ar-Ar-NHAc] and mTAT[SucNH-Ar-Ar-L·Eu] probes in co-incubation with dFFLIPTAT gave similar results but the Eu^{3+} emission appeared lower by visual inspection in the case of mTAT [Eu·L-Ar-NHAc], with the perinuclear autofluorescence more easily discernible. Fig. 10A shows typical 2PM images obtained with each probe using APD detection and band-pass (bp) filtering and recorded in the same conditions (laser power, pixel dwell time ...), the same day. Two detection channels were used: (i) 470–540 nm range (blue channel) that is specific for autofluorescence and (ii) 580–690 nm (red channel) that comprises the two Eu^{3+} $^5D_0 \rightarrow {}^7F_J$ (J = 1 and 2) emission bands but also the red tail of the autofluorescence. A majority of cells show a diffuse emission within the cell in the red channel, with autofluorescence distribution hardly detectable, indicating that Eu^{3+} emission level is above the one of the red-edge of the autofluorescence emission. Fig. 10D quantifies the percentage of cells with diffuse staining as determined by visual inspection. For all conjugates it is above 60% and it increases in the order mTAT[Eu·L-Ar-NHAc] < mTAT[Eu·L-Ar-Ar-NHAc] < mTAT[SucNH-Ar-Ar-L·Eu]. With the latter *ca.* 90% of the cells show an unambiguous diffuse Eu^{3+} staining. The intensity of Eu^{3+} emission vary strongly from cell-to-cell. This is typical of CPP-based luminescent probes.[38] In order to compare the three compounds, a quantitative assessment of Eu^{3+} staining was performed. For this purpose, the mean intensity (red channel) per pixel was measured using ImageJ in *ca.* 80 cells for cells treated with each compound and for cells not incubated with any of the compounds, as a control. It has been reported that CPP-based luminescent probes can adhere to the coverglass of the cell culture chamber providing a background signal outside cells, especially when 2P imaging is done close to the surface.[19,40] Therefore, the background mean intensity per pixel was determined in several (>50) cell-free areas of the approximate size of a cell. Fig. 10B shows the mean intensity per pixel measured in cells and in background areas (Bg) for the three conjugates and in control experiments (Ctrl). First, for the three conjugates, this quantification shows a great dispersion in the staining level among cells, with the mean intensity spanning an order of magnitude. This confirms the visual inspection. For all three conjugates, the staining is significantly higher than the background (P value <0.0001), the staining of the two conjugates with a ter-aryl antenna is similar (P = 0.24) but significantly higher than that of mTAT[Eu·L-Ar-NHAc] with the bi-aryl antenna (P < 0.0001). Note also that the background is also higher in the case of the two ter-aryl antenna-based compounds (P < 0.0001). This suggests an identical behaviour for all conjugates but with an improved emission in the case of the ter-aryl compounds in agreement with their higher brightness. However, a higher cell penetration efficiency cannot be ruled out to explain this higher staining.

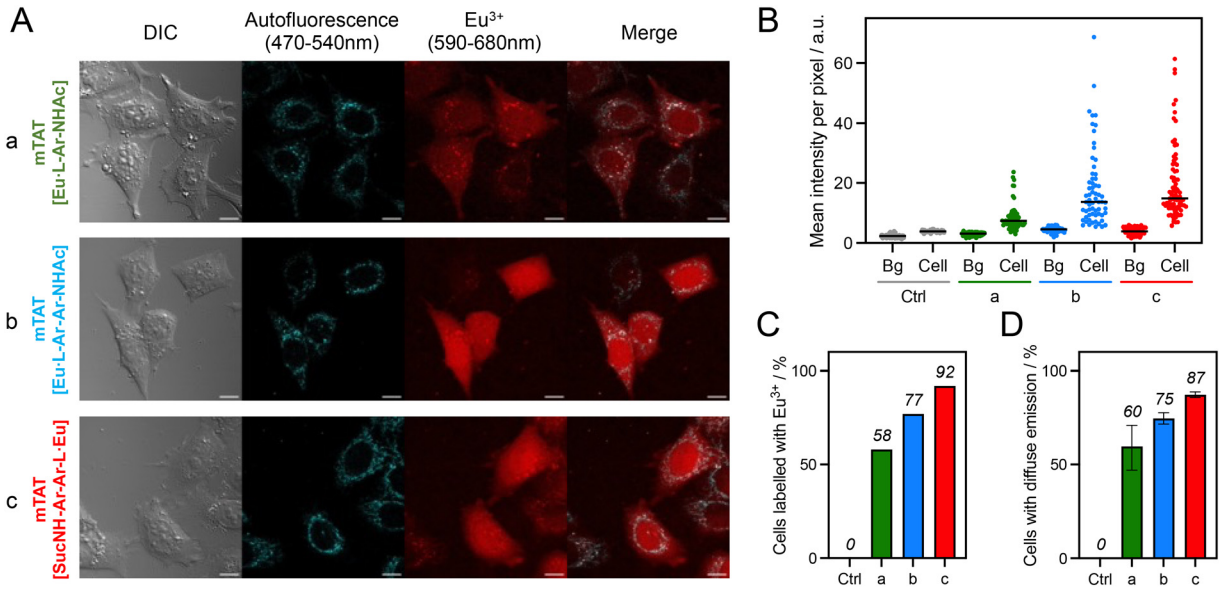

Fig. 10 (A) 2PM imaging (λ_{ex} = 720 nm) of living HeLa cells incubated 1 h with dFFLIPTAT (1.5 μM) and (a) mTAT[Eu·L-Ar-NHAc], (b) mTAT[Eu·L-Ar-Ar-NHAc] or (c) mTAT[SucNH-Ar-Ar-L·Eu] (5 μM) in RPMI medium. From left to right: DIC image, autofluorescence emission (APD, 470–540 nm bp), Eu^{3+} emission (APD, 580–690 nm bp), and merged emission images. (B) Mean intensity per pixel in cells and background (Bg) for the three conjugates and for the control experiment (Ctrl); the black line shows the median value. (C) Percentage of cells unambiguously labelled with Eu^{3+}, determined from the limit of detection. (D) Percentage of cells with diffuse emission, as determined by visual inspection. It was determined by three of the co-authors, the mean is plotted and the range is indicated by error bars.

Finally, the percentage of cells unambiguously stained with the Eu^{3+} probe (Fig. 10C) was determined by counting the cells with a mean intensity per pixel above the limit of detection (LoD) defined by eqn (5),

$$\mathrm{LoD} = < I_{\mathrm{Bg}} > + I_{\mathrm{AF}} + 3 \times \mathrm{SD}(I_{\mathrm{Bg}}) \quad (5)$$

where $<I_{Bg}>$ and $\mathrm{SD}(I_{Bg})$ are the mean value and the standard deviation of the mean intensity per pixel in background areas for experiments performed with the conjugate. I_{AF} is the difference between the mean values of intensity in cells and background areas in the control experiment, corresponding to the intensity of the red tail of the autofluorescence (I_{AF} was measured to be 1.55). For the three conjugates, this percentage increases in the order mTAT[Eu·L-Ar-NHAc] < mTAT[Eu·L-Ar-Ar-NHAc] < mTAT[SucNH-Ar-Ar-L·Eu] and for each conjugate, it matches well the percentage of cells with diffuse emission as determined by visual inspection (Fig. 10D). This indicates that the improvement in the Eu^{3+} emission intensity in the case of the ter-ayl antennae-based conjugates is strong enough to be estimated qualitatively by visual inspection. Overall, these 2P microscopy experiments demonstrate the benefits of switching from a bi-aryl to a ter-aryl antenna for the Eu^{3+} complexes.

The quantitative data presented here allow comparison of two cell internalization strategies relying on (1) TAT dimers, with, on the one hand, dTAT[Eu·L-Ar-NHAc], and (2) TAT monomer + dFFLIPTAT, with, on the other hand, mTAT [Eu·L-Ar-NHAc], both conjugates having the same antenna. The former strategy, with the probe at 5 μM, yielded *ca.* 35% of cells with unambiguous diffuse cytosolic staining of Eu^{3+} (ref. 19) while the latter strategy gave *ca.* 60%, at the same probe concentration, *i.e.* with half the amount of Eu^{3+} complex. This means that superior cytosolic delivery is achieved by co-incubation of the mTAT probe with dFFLIPTAT compared to the dTAT probe. Combining the dFFLIPTAT strategy with a better ter-aryl antenna, enhances even more the number of cells with detectable diffuse staining.

Conclusions

Eu^{3+} based luminescent bioprobes with *p*-amido- or *p*-methoxy–aryl–picolinate antennae (*i.e.* bi-aryl antennae A1 and A2) that we have described previously suffer from a weak absorption above 350 nm. In this article, we have evaluated the benefit of inserting an additional aryl ring within these antennae to red shift the absorption and achieve superior 1P and 2P photophysical properties. Three compounds with ter-aryl antennae, mTAT[Eu·L-Ar-Ar-NHAc], mTAT[Eu·L-Ar-Ar-OMe] and mTAT[SucNH-Ar-Ar-L·Eu], were synthesized and studied, differing in the nature of the electron donating group and/or in the peptide grafting point. From our photophysical study, the best compromise between the red shift of the excitation wavelength and the 2P brightness is compound mTAT [SucNH-Ar-Ar-L·Eu]. The [SucNH-Ar-Ar-L·Eu] complex shows photophysical properties similar to those that can be obtained using the related *p*-alkoxy–aryl–ethynyl–picolinate (antenna A3), which cannot be incorporated into peptide conjugates due to side reactions arising with the alkyne group during peptide synthesis (especially, acidic deprotection treatments).

Comparatively, the ter-aryl antenna is fully stable in peptide synthesis conditions. The increased 2P brightness at 720 nm gained by passing from a bi-aryl antenna to a ter-aryl antenna is likely to be responsible for the better staining and detection achieved with mTAT[SucNH-Ar-Ar-L·Eu] in 2PM experiments. This article demonstrates that the ter-aryl *p*-amido–aryl–aryl–picolinate antenna is an interesting alternative to *p*-alkoxy–aryl–ethynyl–picolinate for the 2P sensitization of Eu^{3+} luminescence.

Author contributions

Conceptualization: O. S., O. M.; investigation: B. C., A. G., L. B., A. N., G. M., S. E., V. M.-F., O. S.; validation: O. S., A. G., A. B., O. M., V. M.-F., D. B., J. K. M.; writing (original draft): O. S.; writing (review & editing): all authors. Visualization: O. S.

Data availability

The data supporting this article have been included as part of the ESI.†

Conflicts of interest

There are no conflicts to declare.

Acknowledgements

Authors acknowledge the Agence Nationale de la Recherche (ANR-18-CE06-0022 and ANR-21-CE29-0018), the Labex ARCANE, CBH-EUR-GS (ANR-17-EURE-0003) and the CEA FOCUS Biomarqueurs program for financial support. Imaging experiments were done on Microcell core facility of the Institute for Advanced Biosciences (UGA – Inserm U1209 – CNRS 5309). This facility belongs to the IBISA-ISdV platform, member of the national infrastructure France-BioImaging supported by the French National Research Agency (ANR-10-INBS-04).

References

1 J.-C. G. Bünzli and S. V. Eliseeva, in *Lanthanide Luminescence*, ed. P. Hänninen and H. Härmä, Springer Berlin Heidelberg, 2011, pp. 1–45.
2 J.-C. G. Bünzli, Lanthanide light for biology and medical diagnosis, *J. Lumin.*, 2016, **170**, 866–878.
3 M. Sy, A. Nonat, N. Hildebrandt and L. J. Charbonnière, Lanthanide-based luminescence biolabelling, *Chem. Commun.*, 2016, **52**, 5080–5095.
4 E. Mathieu, A. Sipos, E. Demeyere, D. Phipps, D. Sakaveli and K. E. Borbas, Lanthanide-based tools for the investigation of cellular environments, *Chem. Commun.*, 2018, **54**, 10021–10035.
5 G.-Q. Jin, Y. Ning, J.-X. Geng, Z.-F. Jiang, Y. Wang and J.-L. Zhang, Joining the journey to near infrared (NIR) imaging: the emerging role of lanthanides in the designing of molecular probes, *Inorg. Chem. Front.*, 2020, **7**, 289–299.
6 I. Martinić, S. V. Eliseeva and S. Petoud, Near-infrared emitting probes for biological imaging: Organic fluorophores, quantum dots, fluorescent proteins, lanthanide(III) complexes and nanomaterials, *J. Lumin.*, 2017, **189**, 19–43.
7 S. I. Weissman, Intramolecular Energy Transfer: The Fluorescence of Complexes of Europium, *J. Chem. Phys.*, 1942, **10**, 214–217.
8 J.-C. G. Bünzli, On the design of highly luminescent lanthanide complexes, *Coord. Chem. Rev.*, 2015, **293**, 19–47.
9 A. D'Aléo, F. Pointillart, L. Ouahab, C. Andraud and O. Maury, Charge transfer excited states sensitization of lanthanide emitting from the visible to the near-infra-red, *Coord. Chem. Rev.*, 2012, **256**, 1604–1620.
10 W. Thor, H.-Y. Kai, Y.-H. Yeung, Y. Wu, T.-L. Cheung, L. K. B. Tam, Y. Zhang, L. J. Charbonnière, P. A. Tanner and K.-L. Wong, Unearthing the Real-Time Excited State Dynamics from Antenna to Rare Earth Ions Using Ultrafast Transient Absorption, *JACS Au*, 2024, **4**, 3813–3822.
11 G. Piszczek, B. P. Maliwal, I. Gryczynski, J. Dattelbaum and J. R. Lakowicz, Multiphoton ligand-enhanced excitation of lanthanides, *J. Fluoresc.*, 2001, **11**, 101–107.
12 M. H. V. Werts, N. Nerambourg, D. Pélégry, Y. L. Grand and M. Blanchard-Desce, Action cross sections of two-photon excited luminescence of some Eu(III) and Tb(III) complexes, *Photochem. Photobiol. Sci.*, 2005, **4**, 531–538.
13 A. Picot, A. D'Aleo, P. L. Baldeck, A. Grichine, A. Duperray, C. Andraud and O. Maury, Long-lived two-photon excited luminescence of water-soluble europium complex: Applications in biological imaging using two-photon scanning microscopy, *J. Am. Chem. Soc.*, 2008, **130**, 1532–1533.
14 G.-L. Law, K.-L. Wong, C. W.-Y. Man, S.-W. Tsao and W.-T. Wong, A two-photon europium complex as specific endoplasmic reticulum probe, *J. Biophotonics*, 2009, **2**, 718–724.
15 A. D'Aléo, A. Bourdolle, S. Brustlein, T. Fauquier, A. Grichine, A. Duperray, P. L. Baldeck, C. Andraud, S. Brasselet and O. Maury, Ytterbium-Based Bioprobes for Near-Infrared Two-Photon Scanning Laser Microscopy Imaging, *Angew. Chem., Int. Ed.*, 2012, **51**, 6622–6625.
16 A. T. Bui, A. Roux, A. Grichine, A. Duperray, C. Andraud and O. Maury, Twisted Charge-Transfer Antennae for Ultra-Bright Terbium(III) and Dysprosium(III) Bioprobes, *Chem. – Eur. J.*, 2018, **24**, 3408–3412.
17 A. T. Bui, A. Grichine, S. Brasselet, A. Duperray, C. Andraud and O. Maury, Unexpected Efficiency of a Luminescent Samarium(III) Complex for Combined Visible and Near-Infrared Biphotonic Microscopy, *Chem. – Eur. J.*, 2015, **21**, 17757–17761.
18 J.-H. Choi, G. Fremy, T. Charnay, N. Fayad, J. Pécaut, S. Erbek, N. Hildebrandt, V. Martel-Frachet, A. Grichine

and O. Sénèque, Luminescent Peptide/Lanthanide(III) Complex Conjugates with Push–Pull Antennas: Application to One- and Two-Photon Microscopy Imaging, *Inorg. Chem.*, 2022, **61**, 20674–20689.

19 K. P. Malikidogo, T. Charnay, D. Ndiaye, J.-H. Choi, L. Bridou, B. Chartier, S. Erbek, G. Micouin, A. Banyasz, O. Maury, V. Martel-Frachet, A. Grichine and O. Sénèque, Efficient cytosolic delivery of luminescent lanthanide bioprobes in live cells for two-photon microscopy, *Chem. Sci.*, 2024, **15**, 9694–9702.

20 J.-H. Choi, A. Nhari, T. Charnay, B. Chartier, L. Bridou, G. Micouin, O. Maury, A. Banyasz, S. Erbek, A. Grichine, V. Martel-Frachet, F. Thomas, J. K. Molloy and O. Sénèque, Carbazole-Based Eu^{3+} Complexes for Two-Photon Microscopy Imaging of Live Cells, *Inorg. Chem.*, 2025, **64**, 2006–2019.

21 A. T. Bui, M. Beyler, Y.-Y. Liao, A. Grichine, A. Duperray, J.-C. Mulatier, B. L. Guennic, C. Andraud, O. Maury and R. Tripier, Cationic Two-Photon Lanthanide Bioprobes Able to Accumulate in Live Cells, *Inorg. Chem.*, 2016, **55**, 7020–7025.

22 S. Mizzoni, S. Ruggieri, A. Sickinger, F. Riobé, L. Guy, M. Roux, G. Micouin, A. Banyasz, O. Maury, B. Baguenard, A. Bensalah-Ledoux, S. Guy, A. Grichine, X.-N. Nguyen, A. Cimarelli, M. Sanadar, A. Melchior and F. Piccinelli, Circularly polarized activity from two photon excitable europium and samarium chiral bioprobes, *J. Mater. Chem. C*, 2023, **11**, 4188–4202.

23 D. Akl, L. Bridou, M. Hojorat, G. Micouin, S. R. Kiraev, F. Riobé, S. Denis-Quanquin, A. Banyasz and O. Maury, Comprehensive Photophysical and Nonlinear Spectroscopic Study of Thioanisolyl-Picolinate Triazacyclononane Lanthanide Complexes, *Eur. J. Inorg. Chem.*, 2024, **27**, e202300785.

24 K. Binnemans, Interpretation of europium(III) spectra, *Coord. Chem. Rev.*, 2015, **295**, 1–45.

25 A. Beeby, I. M. Clarkson, R. S. Dickins, S. Faulkner, D. Parker, L. Royle, A. S. de Sousa, J. A. G. Williams and M. Woods, Non-radiative deactivation of the excited states of europium, terbium and ytterbium complexes by proximate energy-matched OH, NH and CH oscillators: an improved luminescence method for establishing solution hydration states, *J. Chem. Soc., Perkin Trans. 2*, 1999, 493–504.

26 M. H. V. Werts, R. T. F. Jukes and J. W. Verhoeven, The emission spectrum and the radiative lifetime of Eu^{3+} in luminescent lanthanide complexes, *Phys. Chem. Chem. Phys.*, 2002, **4**, 1542–1548.

27 N. Kofod, L. G. Nielsen and T. J. Sørensen, Temperature Dependence of Fundamental Photophysical Properties of $[Eu(MeOH\text{-}d4)_9]^{3+}$ Solvates and $[Eu{\cdot}DOTA(MeOH\text{-}d4)]^-$ Complexes, *J. Phys. Chem. A*, 2021, **125**, 8347–8357.

28 D. Kovacs, E. Mathieu, S. R. Kiraev, J. A. L. Wells, E. Demeyere, A. Sipos and K. E. Borbas, Coordination Environment-Controlled Photoinduced Electron Transfer Quenching in Luminescent Europium Complexes, *J. Am. Chem. Soc.*, 2020, **142**, 13190–13200.

29 A. Weller, Electron-transfer and complex formation in the excited state, *Pure Appl. Chem.*, 1968, **16**, 115–124.

30 W. D. Horrocks, J. P. Bolender, W. D. Smith and R. M. Supkowski, Photosensitized near infrared luminescence of ytterbium(III) in proteins and complexes occurs via an internal redox process, *J. Am. Chem. Soc.*, 1997, **119**, 5972–5973.

31 A. Beeby, S. Faulkner and J. A. G. Williams, pH Dependence of the energy transfer mechanism in a phenanthridine-appended ytterbium complex, *J. Chem. Soc., Dalton Trans.*, 2002, 1918–1922.

32 D. Kocsi, D. Kovacs, J. A. L. Wells and K. E. Borbas, Reduced quenching effect of pyridine ligands in highly luminescent Ln(III) complexes: the role of tertiary amide linkers, *Dalton Trans.*, 2021, **50**, 16670–16677.

33 D. Parker, J. D. Fradgley, M. Delbianco, M. Starck, J. W. Walton and J. M. Zwier, Comparative analysis of lanthanide excited state quenching by electronic energy and electron transfer processes, *Faraday Discuss.*, 2022, **234**, 159–174.

34 P. Luo, E. C. Feinberg, G. Guirado, S. Farid and J. P. Dinnocenzo, Accurate Oxidation Potentials of 40 Benzene and Biphenyl Derivatives with Heteroatom Substituents, *J. Org. Chem.*, 2014, **79**, 9297–9304.

35 Y. Qin and Y. Xia, Simultaneous Two-Photon Fluorescence Microscopy of NADH and FAD Using Pixel-to-Pixel Wavelength-Switching, *Front. Phys.*, 2021, **9**, 642302.

36 R. Cao, H. K. Wallrabe and A. Periasamy, Multiphoton FLIM imaging of NAD(P)H and FAD with one excitation wavelength, *J. Biomed. Opt.*, 2020, **25**, 014510.

37 I. A. Gorbunova, M. K. Danilova, M. E. Sasin, V. P. Belik, D. P. Golyshev and O. S. Vasyutinskii, Determination of fluorescence quantum yields and decay times of NADH and FAD in water–alcohol mixtures: The analysis of radiative and nonradiative relaxation pathways, *J. Photochem. Photobiol., A*, 2023, **436**, 114388.

38 A. Erazo-Oliveras, K. Najjar, L. Dayani, T.-Y. Wang, G. A. Johnson and J.-P. Pellois, Protein delivery into live cells by incubation with an endosomolytic agent, *Nat. Methods*, 2014, **11**, 861–867.

39 J. Allen and J.-P. Pellois, Hydrophobicity is a key determinant in the activity of arginine-rich cell penetrating peptides, *Sci. Rep.*, 2022, **12**, 15981.

40 M. Serulla, P. Anees, A. Hallaj, E. Trofimenko, T. Kalia, Y. Krishnan and C. Widmann, Plasma membrane depolarization reveals endosomal escape incapacity of cell-penetrating peptides, *Eur. J. Pharm. Biopharm.*, 2023, **184**, 116–124.